Modeling of Solitary Pulmonary Nodules in PET/CT images using Monte Carlo Methods

George Tzanoukos, Anastasios Gaitanis, Alexandros Georgakopoulos, Achilleas Chatziioannou, Sofia Chatziioannou, George Spyrou

***Abstract*— The assessment of solitary pulmonary nodules (SPN) is a very difficult task in PET imaging due to adjacent normal structures. Physicians and computational systems as well, would gain benefit if trained to a large number of SPN cases with controlled topological and morphological characteristics. Our objective was to develop a method for the modeling of the solitary pulmonary nodules in CT and PET images. The modeling of SPN was implemented by Monte Carlo methods taking into consideration morphological characteristics, internal features and Standardized Uptake Value (SUV) activity distribution. For the validation of the model, an observer study from three independent medical experts was performed. The reviewers characterized the lesions as simulated or real and finally they classified them as benign or malignant. According to the results of the human observer study a significant percentage of simulated images could not be differentiated from real ones and the simulated class (benign or malignant) was consistent with the observers' classification.**

I. Introduction

THE assessment of solitary pulmonary nodules (SPN) remains a difficult diagnostic task despite the rapid improvement of various imaging modalities. CT and PET are the most common methods for diagnosis of SPN [1]. CT has sensitivity between 95 and 100% and a specificity ranging from 56 to 93% [1]. Furthermore, PET is useful in differentiation between benign and malignant nodules and several investigations have pointed out that can reduce the number of unnecessary thoracotomies for patients with indeterminate SPN [2]. PET alone is not specific and nor sensitive for all cases, especially for those nodules with small size [3].

Manuscript received July 26, 2013.

G. Tzanoukos is with the post-graduate Program: "Information Technologies in Medicine and Biology" (ITMB), Univ. of Athens, TEI of Athens, Biomedical Research Foundation of the Academy of Athens (BRFAA), National Center for Scientific Research (NCSR) "Demokritos", Athens, Greece, CO 13676 Greece (phone: +30-2106597630; fax: +30-2106597629; e-mail: gtzanoukos@bioacademy.gr).

A. Gaitanis is with the Department of Biomedical Technology, Biomedical Research Foundation of the Academy of Athens (BRFAA), Athens, Greece (e-mail: agaitanis@bioacademy.gr).

A. Georgakopoulos is with the Nuclear Medicine Department, Biomedical Research Foundation of the Academy of Athens (BRFAA), Athens, Greece (e-mail: ageorgakop@bioacademy.gr).

A. Chatziioannou is with the First Radiology Department, Aretaieion Hospital, University of Athens, Athens, Greece; (e-mail: achatzi@med.uoa.gr)

S. Chatziioannou is with the Nuclear Medicine Department, Biomedical Research Foundation of the Academy of Athens (BRFAA), Athens, Greece (e-mail: sofiac@bcm.edu)

G. Spyrou is with the Biomedical Informatics Unit, Environmental Health & Biophysics Center, Biomedical Research Foundation of the Academy of Athens (BRFAA), Athens, Greece (Corresponding Author, e-mail: gspyrou@bioacademy.gr).

978-1-4799-3163-7/13/$31.00 ©2013 IEEE

Several groups have studied the ability of PET in detectability of lung tumors. Kadrmas et al [4, 5] used a multi compartment anthropomorphic phantom that is outfitted with numerous lesions of known size and activity concentration. Boellaard et al [6] used an anthropomorphic thorax phantom with inserted tumors, simulated as spheres with various sizes and background ratios. Some other groups have used more sophisticated phantoms, such as the mathematical cardiac torso (MCAT) phantom with added spherical lesions [7].

Stute et al [8] described a method for efficient simulation of PET images of patients with tumors, introducing the realistic modeling of radiotracer heterogeneity. The investigation of lesion detectability and quantification accuracy in whole body PET studies, assessed by Monte Carlo (MC) simulation methods, can be found in [9]. Using MC methods the morphological and internal characteristics of SPN can be modeled very accurately.

Aim of this work is the development of a method suitable for the modeling of various types of SPNs in PET and CT images. The purpose of the modeling is to create images containing realistic SPNs, which will be used in the training of physicians and of computational intelligence systems as well. In the next sections, the characteristics of various SPN types will be described, the Monte Carlo modeling methods will be analyzed and the evaluation of the method through a multi-observer study will be presented.

II. Materials and Methods

A. SPN Image Simulation

For the simulation of SPN several morphological characteristics such as size, margins and contour were taken into consideration. Also, the internal features, such as the presence of patterns of calcification for benign and malignant nodules, were simulated. Approximately 79% of smooth are benign, lobulation occurs up to 75% in benign nodules and finally, about 90% of the SPN with speculated contours can be malignant [10 - 11]. According to the literature, almost 80% of benign nodules have size between 7 and 20 mm [10 - 11]. SPN are either spherical or elliptical and the ratio of the two axes is up to 1.29 [12].

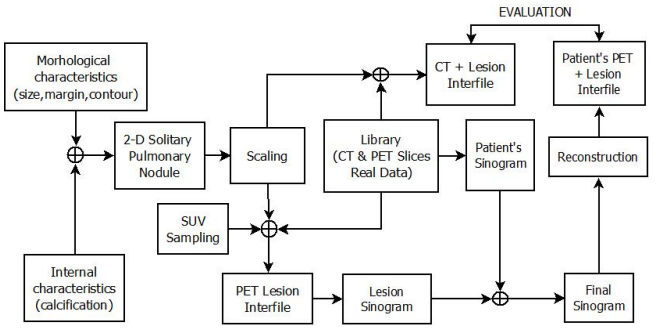

Fig. 1. Algorithm flowchart for SPN image simulation

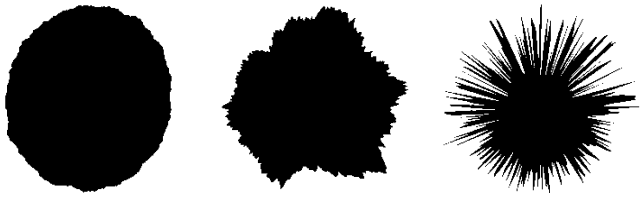

Fig. 2. Simulated 2D images of SPN. The nodule on the left has smooth, well defined border, the middle one has lobulated margin and the lesion on the right has corona radiata border

Our 2D modeling algorithm pipeline is presented in Fig.1. We suppose that it is equally probable for a lesion to be smooth, lobulated or having the appearance of corona radiata. After the Monte Carlo decision concerning the margin of the SPN, and depending on that, the nodule is being characterized as benign or malignant according to the related probabilities. A Monte Carlo decision about the size (diameter) of the SPN also takes place.

In order to produce the proper shape according to our modeling pipeline, we produce fluctuations of the shape radius, depending on the selection made each time, around a fixed point. For example, in the case of a coronal radiata margin the fluctuation is larger and decreases as the lesion becomes smoother. Consequently, the size and shape of the SPN is depicted as a 2D image. Such shape examples are shown in Fig.2.

The internal characteristics of benign and malignant nodules are different. A benign nodule might have central, diffused solid, laminated or popcorn-like calcification. On the other hand, the malignant patterns of calcification are diffused, amorphous, and eccentric or stippled [10-11, 13-14]. For each class (benign and malignant) we consider the four types of calcification as equal probable. The selected calcification is then added to the simulated image of the morphological characteristics, depicting the final 2D image of SPN. The pixel values of each lesion are normalized to the average pixel value of the background region of the CT slice where the SPN is placed.

For the simulation of PET and CT images two different image matrices were used. The dimensions of the first (PET image) were 168x168 with pixel size of about 4.063mm and the dimensions of the second were 512x512 with pixel size of about 0.977mm.

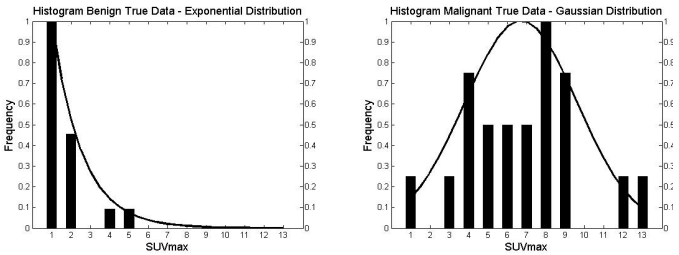

Fig. 3. Histograms derived from the database of 38 patients. The benign histogram follows an exponential distribution and the histogram for the malignant patients follows a gaussian distribution.

SUV is the most employed parameter for the quantitation in PET imaging. The threshold of SUV=2.5 has been used to characterize a lesion as benign or malignant [10]. Therefore the selection of SUV_{max} plays an important role for the characterization of SPN in PET images. In order to model the SUV values accurately, the data from a database of 38 patients were used. These patients were scanned with a Siemens Biograph 6^{TM}, PET/CT. 18 out of 38 nodules were considered by the PET/CT results as benign, whereas the remaining 20 as malignant. The histograms of SUV_{max} values for both groups (benign and malignant) are shown in Fig. 3. As it is obvious the SUV_{max} values of the benign group follow an exponential distribution and those of the malignant group a Gaussian distribution and hence their probability density function (PDF) can be modeled accordingly. In the case of benign nodules the distribution is given by eq. (1),

$$y = f(x \mid \mu) = \frac{1}{\mu} e^{\frac{-x}{\mu}} \tag{1}$$

For malignant nodules the distribution is given by eq. (2)

$$y = f(x \mid \mu, \sigma) = \frac{1}{\sigma\sqrt{2\pi}} e^{\frac{-(x-\mu)^2}{2\sigma^2}} \tag{2}$$

where x is the SUV_{max} value, μ is the mean value and σ is the standard deviation for each class of nodules.

For the optical evaluation of the simulated SPN, the open source Dicom viewer AMIDE was used [15]. In order to reconcile the SPN display with the corresponding one at the diagnostic workstation that the collaborating physicians review the images, the SUV of simulated SPNs were calibrated to eliminate the variations between AMIDE and the workstation (Siemens Syngo) used in clinical diagnosis. To achieve this, the same examination was viewed both from the clinical workstation located at the Nuclear Medicine Department of BRFAA and from AMIDE. The SUV_{max} was measured in clinical viewer and the corresponding value in AMIDE viewer was recorded. The measurements were plotted and were fitted by eq. (3)

$$y = 3{,}858.4x - 590.14 \tag{3}$$

where x is the SUV value and y is the corresponding AMIDE value.

TABLE I
Observers Study - Designation of 120 Cases

Case	S/RC	S/SC	R/SC	R/RC	N/A
1st Observer (NP)	39	61	3	13	4
2nd Observer (NP)	57	41	4	15	3
3rd Observer (R)	62	37	7	13	1

S = Simulated Lesion; RC = Characterized as Real Lesion; SC = Characterized as Simulated Lesion; R = Real Lesion; N/A = No answer

TABLE II
Observers Study – Classification of 100 Simulated Lesions

Case	B/BC	B/MC	M/MC	M/BC	N/A
1st Observer (NP)	68	6	18	1	7
2nd Observer (NP)	75	3	16	4	2
3rd Observer (R)	48	31	14	6	1

B = Benign Lesion; BC = Classified as Benign Lesion; MC = Classified as Malignant Lesion; M = Malignant Lesion; N/A = No answer

TABLE III
Consistency in Repeated Cases

Consistency	1st observer (NP)	2nd observer (NP)	3rd observer (R)
Designation	21/25	20/25	21/25
Classification	20/25	23/25	16/25

B. *Image Reconstruction*

Raw data from five different patients was acquired using a clinical PET/CT scanner (Siemens Biograph 6^{TM}). CT scans were acquired using 130kVp, and ranging mA from 50 to 130.

For the image reconstruction the open source software for PET image reconstruction (STIR) [16] was used. The PET images were forward projected forming projection data of a Biograph 6^{TM} scanner. All images with simulated lesions were also forward projected and the projection data from both the PET images and the simulated lesions were added. Finally, the added projection data were used for the iterative reconstruction using OSEM with 8 subsets and 4 iterations. For the post filtering of the reconstructed image, a 3D Gaussian filter with FWHM at 5mm was employed.

C. *Observer Study*

Three independent observers reviewed the reconstructed images: two nuclear physicians (NP) and one radiologist (R). The observers viewed a transaxial CT slice and the corresponding PET slice. The observers were asked to localize the lesion based on the CT image and then to decide if the SPN is real or artificial according to both images. The observers were also asked to classify the nodules into two classes; probably benign and probably malignant.

The images were viewed using AMIDE software using a MacPro with 2x 2.66 GHz 6-core Intel Xeon having 8 GB RAM and the corresponding 27'' Led Cinema Display.

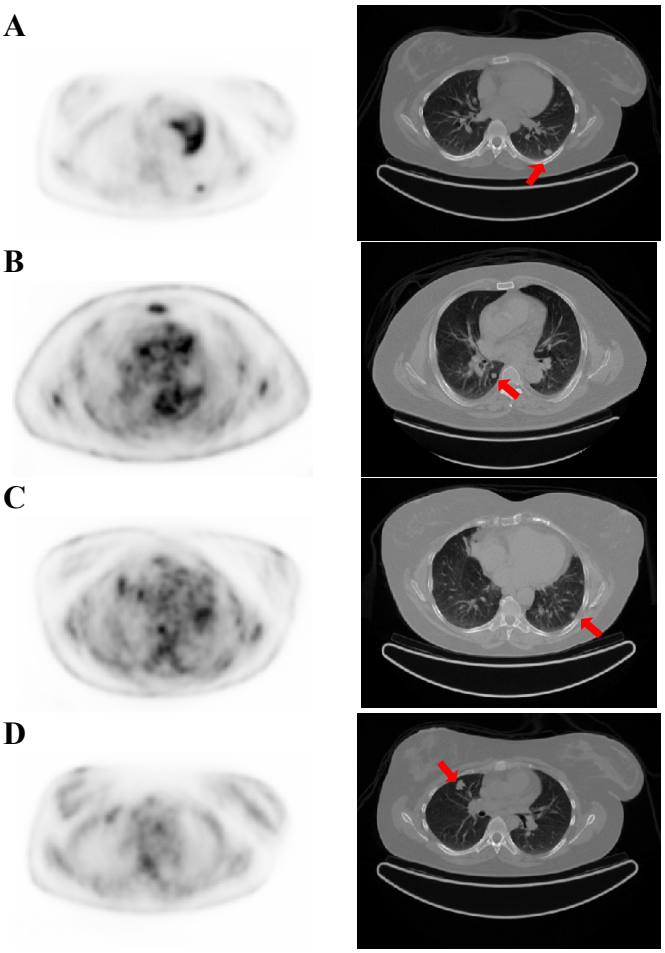

Fig. 3. Transaxial images of CT (right) and the corresponding PET (left). The simulated lesion is indicated with the arrow. A and B illustrate simulated lesions characterized by both observers as real. C and D illustrate simulated lesions characterized by both observers as artificial.

III. RESULTS

A total of 100 SPN containing simulated images were produced by using the high processing power of the BRFAA computing cluster. In this number of simulated cases, the percentage of benignity and malignancy was 80% and 20% respectively. Furthermore, we selected 20 real cases with SPN, 13 of them were benign and 7 malignant. Examples of images with simulated SPN are shown in Fig.3.All the observers localized correctly the SPN in all cases, apart from two. The first observer (NP) designated 39 simulated lesions as real, the second observer (NP) considered 57 simulated nodules to be real and finally the third observer (R) designated 62 simulated nodules as real. Table I lists the results of the evaluation of the observer study for each case, real and simulated.

Moreover, the first two observers (NP) exploited the information given from both the CT and the PET images accomplishing the classification of the simulated lesions as

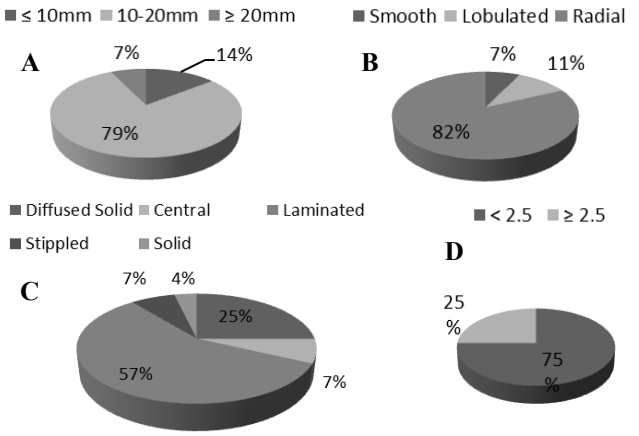

Fig. 4. Characteristics of the 28 simulated cases that all three observers designated as real: lesion size (A), border type (B), calcification (C) and activity concentration (D).

probably benign or probably malignant in high percentage, 86% and 91% respectively, while for the third observer (R) who examined only the CT images the score was 62%. Almost the same results were found when the 120 cases were taken into consideration. The score of three reviewers was 85%, 90% and 63% respectively. The results are presented in Table II.

Among 120 cases, the 25 of them were randomly repeated in order to test the consistency of the reviewers. Twenty of them were with simulated SPN and the rest with real SPN. The results are listed in Table III. We notice that the average for the three reviewers regarding the designation is 83% and the average for the correct classification is 79%. It's worth to be noted that, in 28 cases all of the three observers designated the simulated lesion as real. In Fig. 4 are shown details for allocation of these cases according to the lesion's size, type of the border, internal distribution and activity concentration.

IV. CONCLUSION

Aim of this work is to develop a method for the modeling of the SPN. The modeling is based on the Monte Carlo methods and it was evaluated from three independent physicians showing that 50% of the simulated lesions were reviewed as real. Due to the correct classification on the majority of the cases with a simulated lesion, we educed that we are able to accurately simulate the morphological characteristics and internal features of SPN according to the selected class (benign or malignant).

As template for inserting the simulated SPN we used part of clinical PET/CT scans obtained from patients with no visually detectable tumor or abnormality in the lungs. In the future the method could be more thorough in selecting the appropriate anatomical region so as to present a more realistic total image perspective.

One interesting aspect is that the simulation process appears to be more precise in lesions with size from 10 to 20 mm, corona radiata border, laminated calcification and SUV below 2.5. Considerable effort has been and will be made in the future for the fine insertion of the simulated SPN.

The method described above is expected to be useful for the generation of a large database with various SPNs, with known characteristics, aiming to be the training set in computational intelligence based studies. Furthermore, the implementation of the method could be extended to the creation of 3D SPN.

ACKNOWLEDGMENT

The authors are grateful to A. Panagiotakopoulos and V. Velentzas for their assistance in getting patients' data and K. Karaoglanis for his help about STIR.

REFERENCES

[1] Ost, D. and A. Fein (2004). "Management strategies for the solitary pulmonary nodule." Curr Opin Pulm Med 10(4): 272-278.
[2] Nomori, H., K. Watanabe, et al. (2004). "Evaluation of F-18 fluorodeoxyglucose (FDG) PET scanning for pulmonary nodules less than 3 cm in diameter, with special reference to the CT images." Lung Cancer 45(1): 19-27.
[3] Gould, M. K., G. D. Sanders, et al. (2003). "Cost-effectiveness of alternative management strategies for patients with solitary pulmonary nodules." Ann Intern Med 138(9): 724-735.
[4] Kadrmas, D. J., M. E. Casey, et al. (2009). "Experimental comparison of lesion detectability for four fully-3D PET reconstruction schemes." IEEE Trans Med Imaging 28(4): 523-534.
[5] Kadrmas, D. J. and P. E. Christian (2002). "Comparative evaluation of lesion detectability for 6 PET imaging platforms using a highly reproducible whole-body phantom with (22)Na lesions and localization ROC analysis." J Nucl Med 43(11): 1545-1554.
[6] Boellaard, R., N. C. Krak, et al. (2004). "Effects of noise, image resolution, and ROI definition on the accuracy of standard uptake values: a simulation study." J Nucl Med 45(9): 1519-1527.
[7] Lartizien, C., P. E. Kinahan, et al. (2004). "A lesion detection observer study comparing 2-dimensional versus fully 3-dimensional whole-body PET imaging protocols." J Nucl Med 45(4): 714-723.
[8] Stute S., Vauclin S., Necib H., Grotus N, Tylski P., Rehfeld S.N., Hardey S., Buvat I., (2012). "Realistic and Efficient Modeling of Radiotracer Heterogenity in Monte Carlo Simulations of PET Images With Tumors" IEEE Trans Nucl Sci 59(1): 113-122.
[9] Castiglioni, I., Rizzo, G., Gilardi, M.C., Bettinardi, V. (2005). "Lesion detectability and quantification in PET/CT oncological studies by Monte Carlo simulations." IEEE Trans Nucl Sci 52(1): 136-142
[10] Choromanska, A. and K. J. Macura (2012). "Evaluation of solitary pulmonary nodule detected during computed tomography examination." Pol J Radiol 77(2): 22-34.
[11] Erasmus, J. J., J. E. Connolly, et al. (2000). "Solitary pulmonary nodules: Part I. Morphologic evaluation for differentiation of benign and malignant lesions." Radiographics 20(1): 43-58.
[12] Takashima, S., S. Sone, et al. (2003). "Small solitary pulmonary nodules (< or =1 cm) detected at population-based CT screening for lung cancer: Reliable high-resolution CT features of benign lesions." AJR Am J Roentgenol 180(4): 955-964.
[13] Erasmus, J. J., H. P. McAdams, et al. (2000). "Solitary pulmonary nodules: Part II. Evaluation of the indeterminate nodule." Radiographics 20(1): 59-66.
[14] Choromanska, A. and K. J. Macura (2012). "Evaluation of solitary pulmonary nodule detected during computed tomography examination." Pol J Radiol 77(2): 22-34.
[15] Loening, A. M. and S. S. Gambhir (2003). "AMIDE: a free software tool for multimodality medical image analysis." Mol Imaging 2(3): 131-137.
[16] Thielemans, K., C. Tsoumpas, et al. (2012). "STIR: software for tomographic image reconstruction release 2." Phys Med Biol 57(4): 867-883.